Earth and Planetary Science Letters 482 (2018) 501–509

Contents lists available at ScienceDirect

Earth and Planetary Science Letters

www.elsevier.com/locate/epsl

Control on off-rift magmatism: A case study of the Baikal Rift Zone

Haibin Yang [a,b,*], Zurab Chemia [a], Irina M. Artemieva [a,c], Hans Thybo [c,d]

[a] Department of Geosciences and Natural Resource Management, University of Copenhagen, Øster Voldgade 10, 1350, Denmark
[b] School of Earth Science, University of Melbourne, Parkville, Victoria, 3010, Australia
[c] Eurasia Institute of Earth Science, Istanbul Technical University, Maslak, 34469, Istanbul, Turkey
[d] Centre for Earth Evolution and Dynamics (CEED), University of Oslo, Blindern, 0316, Oslo, Norway

ARTICLE INFO

Article history:
Received 30 April 2017
Received in revised form 14 November 2017
Accepted 16 November 2017
Available online 7 December 2017
Editor: A. Yin

Keywords:
rift graben
pre-existing weak zone
lithosphere heterogeneity
craton
layered rheology
lower crust shearing

ABSTRACT

The Baikal Rift Zone (BRZ) is an active intracontinental rift zone with almost no rift-related magmatism along the rift axis. Most magmatism is observed outside the rift center, and e.g. the major Vitim volcanic field is displaced more than 200 km from the rift center. The reasons for this regional distribution of the magmatism are enigmatic, in particular regarding the off-rift magmatism. We present results of numerical modeling of rift structures similar to BRZ that develop in the transition between craton and orogenic belt. Geophysical evidence suggests that pre-existing weak zones control the location of the BRZ. The models therefore include a pre-set fault (weak zone) within the transition zone between the craton and the orogenic belt as an initial condition in the model. If the pre-existing fault is close to the craton, partial melting in the mantle, due to sub-crustal extension, is offset from the surface rift graben by over 200 km. A horizontal shear zone in the lower crust transfers the extension from the shallow crust to the lithospheric mantle far from the rift graben. A pre-set fault close to the orogenic belt zone is required to explain magmatism close to the rift center in the southernmost BRZ. We conclude that the location of the pre-existing fault zone relative to a change in lithosphere thickness may shift the magmatism away from the surface expression of the rift graben and may explain the location of the off-rift magmatism, e.g. the basaltic Vitim plateau. The predicted geometry of the sedimentary graben along the rift strike is consistent with seismic observations in the northern and central BRZ.

1. Introduction

The Baikal Rift Zone (BRZ) is located between the southeastern edge of the Siberian craton and the Sayan–Baikal fold belt (Fig. 1). Rifting at the BRZ began in the Oligocene (30–35 Ma) as 'slow rifting' which lasted ca. 30 Myr (until the Early Pliocene). The second stage of rifting (Late Pliocene to Quaternary) is characterized by accelerating basin subsidence and rift shoulder uplift and is considered as the 'fast rifting' stage (Logatchev and Zorin, 1987).

In general, massive magmatism due to decompression partial melting is expected in rift zones (Reid and Jackson, 1981). Extensional rift centers usually develop in the most extensively stretched part of the lithosphere and therefore magma eruptions are expected in the rift center, but the BRZ is an exception (Kiselev et al., 1987; Maccaferri et al., 2014). Three main volcanic fields have developed at the BRZ since the Miocene: (1) in and around the Tunka basin and the Khamar-Daban range; (2) in the Vitim plateau to the east of BRZ; (3) in the Udokan area in the northeast (Fig. 1). No magma eruption events have ever been recorded in the rift axis, except for small eruptions in the Tunka depression at the SW end of the BRZ (Kiselev et al., 1987; Logatchev and Zorin, 1987). The volcanic fields of the Khamar-Daban, the Udokan and the Vitim plateau are all off-axis where the latter is offset from the axial rift by more than 200 km (Fig. 1).

Previous studies link the off-rift location of the volcanic fields to (1) lithosphere-scale low-angle detachment faults (Bosworth, 1987), (2) flexure-induced extension at the footwall of rift master faults (Ellis and King, 1991), or (3) gravitational unloading in the crust (Maccaferri et al., 2014). However, these models are not satisfactory for the BRZ because (1) no deeply-penetrating faults down to the lithosphere–asthenosphere boundary have been imaged by geophysical surveys (Nielsen and Thybo, 2009; Thybo and Nielsen, 2009); (2) the off-rift volcanoes appear to occur in the hanging wall rather than the footwall (Fig. 1); (3) crustal unloading itself cannot explain the volcano distribution variation along the rift strike (Fig. 1). There is indication that thick continental lithosphere (>100 km) might not allow magmatism in the rift (Bialas et al., 2010; Buck, 2006). However, even if magmatism does not

* Corresponding author at: School of Earth Science, University of Melbourne, Parkville, Victoria, 3010, Australia.
E-mail address: haibiny@student.unimelb.edu.au (H. Yang).

https://doi.org/10.1016/j.epsl.2017.11.040
0012-821X/

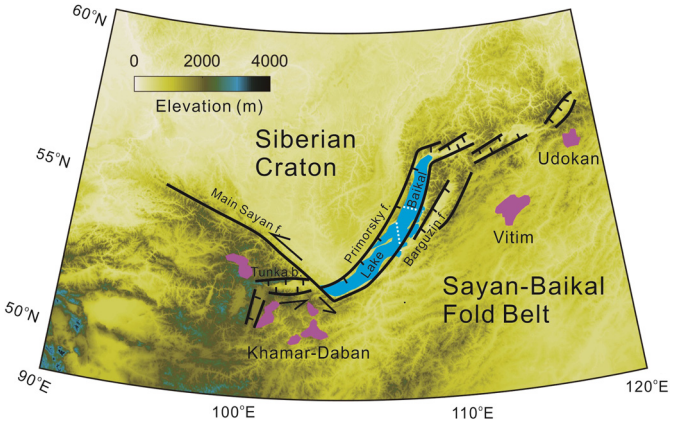

Fig. 1. Map of topography and tectonic setting of the Baikal Rift Zone (BRZ). Faults are named by 'f'. Udokan, Vitim, and Khamar-Daban are three main volcanic fields (red patches, after Kiselev et al., 1987). Black lines roughly mark major tectonic faults (after Sherman, 1978). The white dashed lines across the North and South Baikal lake are two seismic reflection profiles shown in Fig. 5. No magmatism has been recorded along the rift axis since the beginning of stretching at 35–30 Ma except in the Tunka depression. The Vitim volcanic field is located ca. 200 km from the rift axis. (For interpretation of the references to color in this figure, the reader is referred to the web version of this article.)

assist faulting in a rift, synchronous magmatism should not automatically occur far away from the rift center, especially in the presence of a weak zone.

It is commonly recognized that the deformation of the BRZ is guided by inherited weak zones around the suture between craton and orogenic belt (Corti et al., 2011; Petit et al., 1998; Sherman, 1978). The major faults include the Main Sayan fault (>1000 km long) along the southern edge of the Siberian craton, the Primorsky fault bounding the Lake Baikal to the west as a master fault, and the 200 km long Barguzin major fault east of the North Baikal basin (Fig. 1) (Sherman, 1978). Since their initial formation in the early Paleozoic, the faults have been repeatedly reactivated (Konnikov et al., 1993). The role of a pre-existing fault in forming a narrow and deep basin, as is observed in the BRZ, has been tested by analog models (Corti et al., 2011).

In this work, we use numerical geodynamic modeling to investigate the effect of the position of a pre-existing fault on the distribution of volcano eruption centers. Melting processes in the mantle are simulated assuming a batch melting model (Katz et al., 2003), and the modeled melt fractions are compared to local petrological records. In addition, we validate the results of the dynamic processes in the rift zone by comparing predicted rift graben geometry with seismic reflection profiles across the sedimentary basins of the BRZ.

2. Method

2.1. Governing equations

A new 2D finite difference code with a marker-and-cell technique is applied here to simulate the thermomechanical deformation of the crust and upper mantle. We first solve the equations for conservation of mass (1) and momentum (2):

$$\nabla \cdot u = 0 \tag{1}$$

$$\nabla \cdot \sigma' - \nabla P + \rho g = 0 \tag{2}$$

where u is velocity, σ' is deviatoric stress, P is dynamic pressure, ρ is density, and g is gravitational acceleration ($g_x = 0$ and $g_y = 9.81\ \mathrm{m\,s^{-2}}$ for 2D model). For the equation of conservation of mass (1), we assume an incompressibility condition so that changes in density (e.g., due to pressure, temperature, and phase changes) are negligible. To simulate changes in temperature caused by heat transfer, we solve the heat conservation equation

$$\rho c_p \left(\frac{\partial T}{\partial t} + u \cdot \nabla T \right) - \nabla \cdot k \nabla T - H = 0 \tag{3}$$

where c_p is heat capacity, k is thermal conductivity and H is heat production due to radioactive, shear, adiabatic and latent heat sources. The governing conservation equations, of mass, momentum, and energy are solved in the Eulerian frame and material physical property is transported by Lagrangian markers which move in the velocity field interpolated from a fixed Eulerian grid (Gerya, 2009).

2.2. Rheology

The model simulates a visco-elasto-plastic rheology. The elastic material follows Hooke's law for a 2D continuum. For viscous flow, we include the power law dislocation creep

$$\dot{\varepsilon} = A(\sigma')^n \exp\left(-\frac{E + VP}{RT} \right) \tag{4}$$

where $\dot{\varepsilon}$ is strain rate, A is a material constant, σ' is differential stress (the difference between maximal and minimal), n is stress exponent ($n = 1$ for diffusion creep and $n > 1$ for dislocation creep), E is activation energy, V is activation volume, R is the gas constant, and T is temperature. We can reformulate equation (4) to obtain the effective viscosity

$$\eta = \frac{\sigma_{\mathrm{II}}}{2\dot{\varepsilon}_{\mathrm{II}}} \tag{5}$$

where σ_{II} is the second invariant of the deviatoric stress, and $\dot{\varepsilon}_{\mathrm{II}}$ is the second deviatoric strain rate invariant of viscous part of deformation. The effective viscosity is cut at 10^{25} Pa s and 10^{18} Pa s. The Navier–Coulomb yield criterion is used for frictional-plastic deformation when stress reaches a specific limit that marks the transition from viscous to plastic failure (Byerlee, 1978)

$$\sigma_{\mathrm{yield}} = P \sin\phi + C \tag{6}$$

where σ_{yield} is the maximum second deviatoric stress invariant, P is pressure, $\sin\phi$ is friction coefficient and C is cohesion. We follow numerical implementation of eqs. (1)–(6) as described by Gerya (2009).

2.3. Free surface

A free surface condition at the boundary between rock surface and air may have significant effect on lithospheric and mantle dynamics (Kaus and Becker, 2008). It is implemented by introducing a low-density ($1000\ \mathrm{kg\,m^{-3}}$), low viscosity ($10^{18}$ Pa s) near-surface layer. Subsequently, the interface between the markers defining the crust and the air behaves similar to a free surface. In order to obtain meaningful results, the following criterion should be satisfied for the top weak layer (Crameri et al., 2012):

$$\frac{\eta_{st}/\eta_{ch}}{(h_{st}/L)^3} \ll 1 \tag{7}$$

where η_{st} and h_{st} are viscosity and thickness of the weak layer, and η_{ch} and L are the characteristic mantle viscosity (which controls topography relaxation) and the length scale of the model, respectively.

2.4. Erosion and sedimentation

The interface between the weak layer, representing air, and the top of the crust is regarded as an erosion and sedimentation surface, where the evolution is based on the transport equation (Kooi and Beaumont, 1994)

$$\frac{\partial h}{\partial t} = v_y - v_x \frac{\partial h}{\partial x} + \frac{\partial}{\partial x}\left(k_s \frac{\partial h}{\partial x}\right) \tag{8}$$

where k_s is the 'topography diffusion' coefficient, h is the vertical position of the crust topmost surface, v_y and v_x are vertical and horizontal velocity vectors at the surface, respectively. We apply a simplified erosion–sedimentation model, which describes short-range surface processes. Equation (8) can be used to describe surface processes that include downhill diffusion and fluvial erosion. Without better constraints in this study, k_s is chosen as a constant value of 25 $m^2\,yr^{-1}$, which produces reasonable volumes of sediment to accord with geological studies in the BRZ (e.g., $k_s = 1\ m^2\,yr^{-1}$ corresponds to erosion–sedimentation rates of 0.001 $mm\,yr^{-1}$ for a relief of a 1 km height with a wavelength of 200 km). Parameters used for equations (1)–(8) are summarized in Table 1.

2.5. Partial melting

Partial melting and crystallization of the lower crust and the upper mantle are expressed by a simple approximation similar to Gerya and Burg (2007). However, instead of a linear approximation between melt fraction and temperature we use an power function and let the total melt fraction depend on bulk water content (Katz et al., 2003).

$$\begin{aligned}
&F = 0 \quad \text{at } T \le T_{\text{solidus}};\\
&F = \left(\frac{T - (T_{\text{solidus}} - \Delta T)}{T_{\text{liquidus}} - T_{\text{solidus}}}\right)^{\beta_1} \quad \text{at } T_{\text{liquidus}} > T > T_{\text{solidus}},\\
&\quad \text{where } \Delta T = K\left(\frac{X^{\text{bulk}}_{H_2O}}{D_{H_2O} + F(1 - D_{H_2O})}\right)^{\gamma};\\
&F = 1 \quad \text{at } T > T_{\text{liquidus}};
\end{aligned} \tag{9}$$

where F is the melt fraction, $X^{\text{bulk}}_{H_2O}$ and D_{H_2O} ($D_{H_2O} = 0.01$) stands for bulk water content and partitioning coefficient, β_1 and γ are power exponents which are set to 1.5 and 0.75 respectively, and pre-factor $K = 43\,^{\circ}C\ \text{wt.}\%^{-\gamma}$. Mantle solidus temperature for a given pressure is $T_{\text{solidus}} = 1085.7 + 132.9P - 5.1P^2$ and the liquidus temperature is $T_{\text{liquidus}} = 1475.0 + 80.0P - 3.2P^2$, where T is in °C and P is in GPa (Katz et al., 2003). The effective density of partially molten rocks is calculated as $\rho_{\text{eff}} = \rho_{\text{solid}} - F(\rho_{\text{solid}} - \rho_{\text{melt}})$ where densities of solid rock and melt vary with temperature and pressure according to $\rho_{P,T} = \rho_0(1 - \alpha(T - T_0))\ (1 + \beta(P - P_0))$. ρ_0 is the standard density at $P = 0.1$ MPa and $T = 273$ K; α and β are thermal expansion and compressibility coefficients, respectively. ρ_{melt} for sediment and upper crust is set to be 2400 $kg\,m^{-3}$ while other materials have ρ_{melt} of 2700 $kg\,m^{-3}$. A constant value of 10^{18} Pa s is used here as the effective viscosity for molten rocks.

3. Model setup

A 2D finite difference code with visco-elasto-plastic rheologies recently developed by one of us (Z. Chemia) is used to model thermo-mechanical deformation in the lithosphere and describe main evolutionary features of the BRZ. The model domain has dimensions of 800 km × 400 km with 401 × 201 computational

Table 1
Material parameters at $T_0 = 0\,^{\circ}C$ and $P_0 = 10^5$ Pa. Other parameters: H_r radioactive heat production; μ: shear modulus; Molten material occurs when temperature reaches solidus.

Material	Density				Flow law				Yield criteria[4]		Conductivity[5]				Shear modulus
	$\rho_0[1-\alpha(T-T_0)][1+\beta(P-P_0)]$				$\dot{\varepsilon} = A*(\sigma')^n*\exp[-\frac{E+VP}{RT}]$				$\sigma_{\text{yield}} = C + \sin(\phi)P$		$k_0 + q/(T+77)$				
	ρ_0 ($kg\,m^{-3}$)	α (10^{-5} K^{-1})	β (10^{-11} Pa^{-1})	η_0 (Pa s)	A (MPa^{-n} s)	n	E ($kJ\,mol^{-1}$)	V ($cm^3\,mol^{-1}$)	C (MPa)	$\sin(\phi)$	k_0 ($W\,mK^{-1}$)	a (K)	c_p ($JK^{-1}\,kg^{-1}$)	H_r[6] ($\mu W\,m^{-3}$)	μ (GPa)
Water	1000	0	0	1E+18	0	0	0	0	0	0	300	0	3000	0	1E+11
Sediment	2400	3	1	–	0.00032[1]	2.3	154	0	10	0.6	0.64	807	1000	1.3	10
Upper crust	2700	3	1	–	0.00032[1]	2.3	154	0	50	0.6	0.64	807	1000	1	25
Middle crust	2800	3	1	–	0.000332831	3.2	240	0	50	0.6	1.18	474	1000	0.4	30
Lowe crust	2950	3	1	–	0.01[2]	3.2	244	0	50	0.6	1.18	474	1000	0.1	30
Lithosphere	3300	3	1	–	1.58E+04[3]	3.5	530	18	50	0.6	0.73	1293	1000	0.01	65
Asthenosphere	3300	3	1	–	1.58E+04[3]	3.5	530	18	50	0.6	0.73	1293	1000	0.004	65
Weak seed	2700	3	1	–	0.00032	2.3	154	0	25	0.3	0.64	807	1000	1	25
Melt	2400–2700	3	1	1E+18	0	0	0	0	0	0	–	–	–	–	–

[1] Ranalli (1995);
[2] Wang et al. (2012);
[3] Hirth and Kohlstedt (2003);
[4] Byerlee (1978);
[5] Clauser and Huenges (1995);
[6] Artemieva and Mooney (2001).

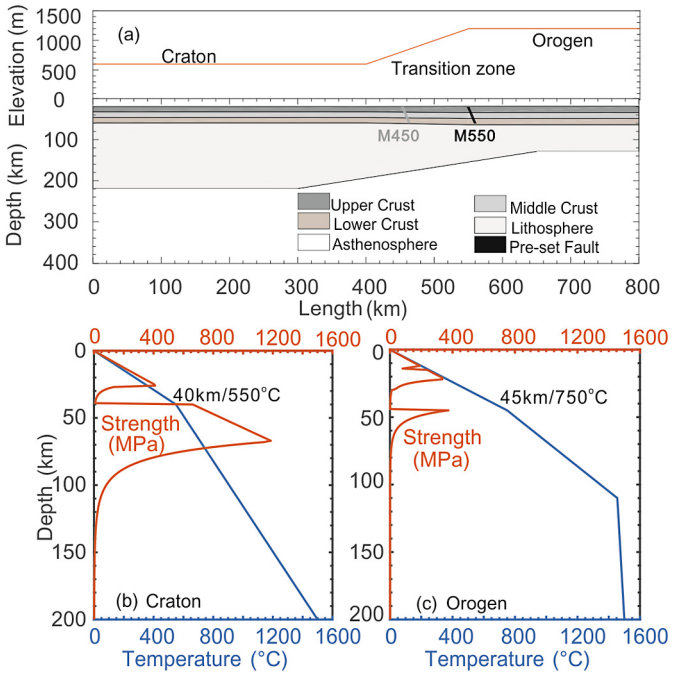

Fig. 2. Initial model: topography and geometry of different layers (a) and initial yield strengths for (b) cratonic and (c) orogenic belt parts of the model. The initial model has no sediment layer but the model allows for erosion and sedimentation during extension. Initial crustal thickness and temperature profiles are linearly interpolated between the craton and the orogenic belt across the transitional zone. To test how the position of a pre-existing fault affects the rifting dynamics, we present results for fault locations at 550 km (M550, black thick line) and 450 km (M450, grey thick line). (For interpretation of the references to color in this figure, the reader is referred to the web version of this article.)

Table 2
Geometry and temperature background parameters in the initial model. The upper, middle, and lower crustal thicknesses are 1/3 of the total crustal thickness. The asthenosphere domain below the lithosphere asthenosphere boundary (LAB) has an adiabatic temperature gradient of 0.5 °C km^{-1}.

	Siberian craton	Sayan–Baikal fold zone
Surface elevation (m)	600	1200
Crustal thickness	40	45
Lithosphere thickness	200	110
Crustal width	400 (0–400)	250 (550–800)
Lithosphere width	300 (0–300)	150 (650–800)
Surface temperature (°C)	0	0
Bottom temperature (°C)	1600	1600
Moho temperature (°C)	550	750
LAB potential temperature (°C)	1400	1400

nodes (Fig. 2, Table 2). The top 20 km of the model is filled with low viscosity (10^{18} Pa s) and low density (1000 kg m^{-3}) material to simulate a free surface (Crameri et al., 2012). The model includes a three-layered crust with a total thickness of 40 km for the cratonic part of the BRZ and 45 km for the Sayan–Baikal orogenic belt (Cherepanova et al., 2013; Thybo and Nielsen, 2009) (Fig. 2, Table 2). The Moho temperature is 550 °C and 750 °C for the craton and orogenic belt, respectively (Artemieva and Mooney, 2001). The thermal lithosphere base is assumed to be 200 km deep at the edge of the craton, and 110 km in the orogenic belt. We assume a potential temperature of 1400 °C and an adiabatic gradient of 0.5 °C km^{-1} in the asthenosphere. Although the lithosphere and asthenosphere have the same rheology (olivine) and density (3300 kg m^{-3}), a chemical lithosphere is designed with higher heat generation rate than the asthenosphere (Table 1). Initially, the thermal lithosphere coincides with the chemical lithosphere, but the thermal and chemical lithosphere will evolve in different ways with time.

Continental upper mantle shows a broad range of water content, ranging from 0 to 170 ppm H_2O in different tectonic settings (Wang, 2010), and a high water content in olivine (6–323 ppm) has been reported for the Udachnaya pipe of the Siberian craton (Doucet et al., 2014). Given that olivine makes <70% of the upper mantle, we select 400 ppm for bulk water content. The remaining rocks after melting tend to be strengthened because of depletion and dehydration (Hirth and Kohlstedt, 1996), but this effect is neglected for simplicity. The molten material is assigned a constant viscosity of 10^{18} Pa s.

The initial model setup includes the presence of a lithosphere-scale transition zone between the craton and the orogenic belt with only a minor change in the Moho depth as supported by regional seismic data (Nielsen and Thybo, 2009; Thybo and Nielsen, 2009) and with a gradual step in the lithosphere thickness from the craton edge to the orogenic belt. The geometry of the transition is based on regional gravity (Petit and Deverchere, 2006), thermal and seismic tomography models (Emmerson et al., 2006), which suggest that the transition is sharper in the southern part of the BRZ, while the northern part of the Baikal basin is still underlain by a thick moderately depleted cratonic lithosphere (Artemieva, 2009).

To test the effect of the pre-set fault position on regional dynamics, we compare the simulated results for two identical initial models except for the fault position which is set at $x = 450$ km and $x = 550$ km, referred to as M450 and M550. In our two modes, rifting is modeled by introducing a 3 km wide fault in the initial model, which is subject to constant extension rates (two stages: slow, 2 mm yr^{-1} (0–20 Myr), and fast, 4 mm yr^{-1} (20–31 Myr)) applied to the right boundary, while the top and the left boundaries are free slip. The pre-existing fault penetrates through the crust but not into the mantle. The extension rate is consistent with present day GPS data, which shows that the southern and the central parts of the rift are opening at a rate of 4.5 ± 1.2 mm yr^{-1} in an NW-SE direction that is almost orthogonal to the local rift direction (Calais et al., 1998). The depth range is justified by regional seismicity which shows very few sub-Moho earthquakes (Deverchere et al., 2001). The fault dip is set to ∼75° towards the orogenic belt. The strength of the weak material in the fault zone, both cohesion (25 MPa) and friction coefficients (0.3), are half of the normal crust. The M450 model places the pre-existing fault 100 km closer to craton than the M550 model, such that the weak zone in M450 is overlying a thicker and stronger lithospheric mantle than that in M550.

4. Results

Within 31 Myr of model time, the two models M450 and M550 lead to significant differences in (1) lithosphere deformation styles and (2) relative distances between the melting center in the mantle and the graben in shallow crust.

4.1. Lithosphere deformation

Once extension is applied to the models, the pre-set faults work as weak zones that localize deformation in the crust (Fig. 3a and d). However, this initial deformation pattern evolves differently with time for M450 and M550. For the M450 model, the pre-set fault functions as a master fault through the entire evolution without significant changes of the fault shape (Fig. 3a, b and c), although the orogenic belt of the model gradually becomes subject to uniform extension. In contrast, the master fault in M550 migrates from $x = 550$ km to $x = 600$ km, and the initial hanging wall is slightly strained by 22 Myr (Fig. 3e) after which the right flank of the graben becomes heavily deformed to form a necking zone with a strong mantle upwelling approaching its rift flank (Fig. 3f).

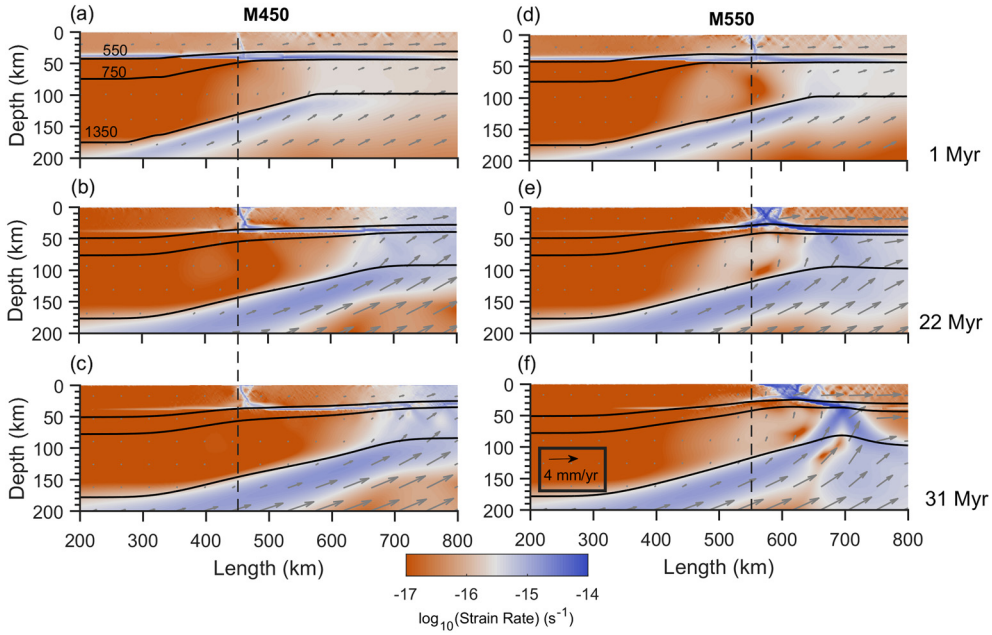

Fig. 3. Snapshots of strain rate for the model M450 (a, b, c) and the model M550 (d, e, f) after ca. 1, 22 and 31 Myr of extension. Black solid lines are isotherm lines of 550, 750, and 1350 °C; dashed lines mark the position of initial weak zones; grey arrows show velocity field with the same scaling (insert box in f). Model M450 initially localizes deformation in the pre-existing weak zone, but the orogenic section is gradually extended at later stage. In contrast, model M550 localizes strain at the inherited fault, and the master fault migrates towards the orogenic belt to form one necking zone with passive mantle upwelling. (For interpretation of the references to color in this figure, the reader is referred to the web version of this article.)

This kind of migration of the master fault is consistent with the present seismicity which is localized at the eastern flank of the south and central Lake Baikal (Petit and Deverchere, 2006).

The different evolution patterns may be attributed to the mantle strength beneath the inherited weak zone. For a pre-set fault overlying a cold and strong cratonic lithospheric mantle (M450) (Fig. 3a), the 550 °C isotherm in the cratonic lithosphere drops from a depth of 40 km (1 Myr) to 50 km (31 Myr) below surface, indicating that cooling dominates the temperature regime in the area adjacent to the preset fault. Cooling and strengthening of the cratonic lithosphere around the localized rift zone make it resistant to deformation, and therefore stretching is accommodated within a weak orogenic lithosphere which starts to be uniformly extended. In contrast with the surface deformation, the lithospheric mantle directly beneath the BRZ is too strong to be extended, but the thinner lithosphere further to the east (right) is sufficiently weak e to extend. The rightward motion of the right boundary including the mantle and crust is drawing relatively diffuse mantle flow from the base up toward the right. The diffuse extension and thinning of orogenic lithosphere enhances the upward component of mantle flow (Fig. 3b and c). The 1350 °C isotherm in the orogenic mantle uplifts from 97 km (1 Myr) to 81 km (31 Myr) depth. Increasing temperature, together with enhanced extension, forms a positive feedback system, which weakens the orogenic lithosphere thermo-mechanically. Further, both increasing temperature and extension trigger decompressional melting which contributes to mantle melting below the orogenic belt (Fig. 4b and c). The offset of extension is accommodated by a horizontal shear zone in the lower crust, which transfers the extension from the crustal BRZ in the west to the sub-crustal mantle lithosphere in the east.

Only one normal fault develops when the preset fault is close to the craton in M450. The reason is that the strength of the lithosphere increases towards the craton which has colder lithosphere than the orogenic belt. It will be hardly possible to have another fault on the craton side. In the orogenic part, the lithosphere is thinner than the cratonic lithosphere, the brittle crust is 30 km thick and the inherent cohesion is 50 MPa (Fig. 1). This rheology requires high bending forces to offset the fault, so that stress around the fault exceeds yield stress and therefore another fault forms (Lavier et al., 2000), with the result that multiple faults form in the orogenic belt. Continuing stretching of the orogenic belt will eventually form a narrow rift with lithosphere necking (Buck et al., 1999). This process is not modeled here because it has not been observed in the BRZ.

In contrast, the pre-set fault in the M550 model is outside of the craton and overlies a relatively weak mantle (Fig. 3d). At the early stages of rifting, the lithosphere extension lowers topography and uplifts the underlying mantle due to low pressure in the rift zone (Fig. 4d, e and f). Crustal thinning will increase the regional thermal gradient, thus further reducing the crustal strength. This positive feedback prevents propagation of lithosphere deformation into the orogenic belt (Fig. 3e). While the orogenic lithosphere in M450 becomes subject to gradual uniform extension (Fig. 3b), the orogenic crust in model M550 remains almost intact from deformation by the intensive extensional strain (Fig. 3e). As in M450, crustal deformation cannot propagate leftwards into the craton due to the high strength of the cratonic lithosphere. Finally, at the later stages of rifting, the lithosphere becomes weakest between the preset fault ($x = 550$ km) and the western edge of the orogenic belt ($x = 700$ km), and lithosphere necking localizes in this restricted zone (Fig. 3f).

4.2. Melt generation

During the first 20 Myr for both the M450 and M550 models, almost no melt is generated and there is no more than 0.5 wt.% molten material at a depth of 100 km (Fig. 4). Both models show that the pre-defined fault tends to localize crustal deformation to evolve into a rift graben at the surface (Figs. 3a, d and 4), which we refer to as the rift center (particle marked by dark blue in Fig. 4). During the second stage of rifting with a 4 mm yr^{-1} extension rate, intensive decompression partial melting takes place due to a higher extension rate. However, the two models (M450 and M550) have different relative distances between the melt cen-

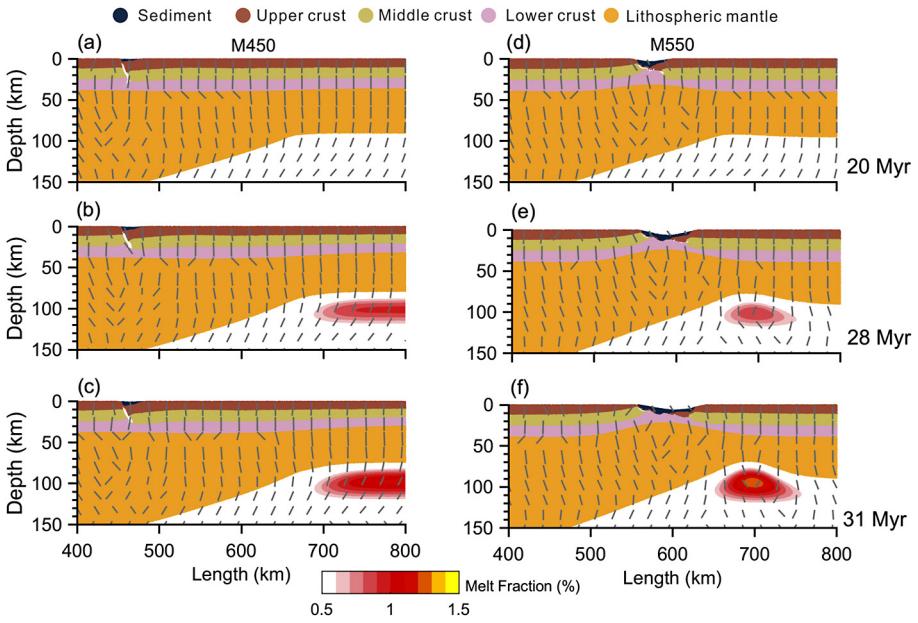

Fig. 4. Snapshots of the evolution of the model M450 (a, b, c) and the model M550 (d, e, f) after 20, 28 and 31 Myr. Color patches in the asthenosphere (white background) show partial melt fraction; grey bars show the direction perpendicular to the maximum extensional stress direction which is assumed to cause potential fractures for magma intrusion. Dark blue material on the surface close to pre-set fault (narrow white) outlines the rift graben. Decompressional adiabatic melting occurs in the asthenosphere assuming a wet peridotite composition with 0.04 wt.% water. For M450 (b and c), the partial melting center in the mantle is at ca. $x = 700$–800 km which is more than 250 km from the rifting center while partial melting in the model M550 is located relatively close to the rifting center at 100 km distance. (For interpretation of the references to color in this figure, the reader is referred to the web version of this article.)

ter in the mantle and the rift graben. In the M550 model, mantle upwelling takes place at $x = 650$–750 km (close to the rift center) (Fig. 4), corresponding to the lithosphere necking zone in the mantle (Fig. 3f). At 28 Myr, the zone of partial melting is 25–30 km thick with a maximum melt fraction of around 0.8% (Fig. 4). At 31 Myr, the partially molten zone with 1.4% of melt has a triangular shape with a horizontal size of 100 km and a height of 40 km, and is located below the right flank of the rift (Fig. 4). In contrast, the M450 model has a molten zone with dimensions of 100 km horizontally and 20 km vertically with 1% melt fraction at 28 Myr. It is located at $x = 700$–800 km which is about 300 km away from the rift center which is located at $x = 450$ km (Fig. 4). At 31 Myr, the maximum melt fraction reaches 1.2 wt.% at a depth of ca. 80 km and still 200–300 km away from the rift center (Fig. 4). The melt location in M450 is determined by the moderately extended lithosphere in the orogenic section (Fig. 3).

Partial melting in the M550 model occurs near the rift center and its flank (Fig. 4). This is consistent with observations in the southwestern BRZ with rift-related basalts in the Tunka basin and the Khamar-Daban range (Logatchev and Zorin, 1992). The off-rift partial melting in M450 is consistent with observations in the Vitim volcanic field. Based on geochemical studies in the Vitim province, Johnson et al. (2005) suggested that alkali and tholeiitic basalts are products of high degree adiabatic decompression (up to 7%) of fertile peridotite at depths between 85 km and 115 km with an adiabatic potential temperature as high as ~1450 °C. This melting depth interval corresponds to our numerical results for the M450 model, but we predict a smaller melt fraction (Fig. 4). According to theoretical models of partial melting (Mckenzie and Bickle, 1988), a very small stretching factor ($\beta = 1.5$) can produce between ~3 km and ~7 km of melt thickness, respectively, for a 100-km-thick and 70-km-thick mechanical boundary layer at 1480 °C. In the BRZ, a total of <6000 km^3 of magmatic rocks cover areas of 40000 km^2 (~30000 km^2 in Khamar-Daban, 7000 km^2 in Vitim and 3000 km^2 in Udokan) (Logatchev and Florensov, 1978) corresponding on average to a 0.15 km thick basaltic layer. Although there is no direct survey for the volume of intrusions in the Vitim pleteau, the ratio of intrusive versus eruptive melt volume for intracontinental volcano fields is estimated to vary between 4:1 and 10:1 (Crisp, 1984). The distribution and prediction are consistent with our numerical results which indicate a 1–2% melt fraction. The observed stretching factor at Lake Baikal is 1.3–1.7 (Thybo and Nielsen, 2009), and it is estimated that the thickness of intrusive material is ca. 7 km in a ~70 km wide zone. Such thick intrusive underplating might reflect a complex pattern of magma migration. This process is beyond the discussion of our 2D model. Numerical experiments do not show waning in the volcanic activity as reported for the BRZ. This may be attributed to tectonic stress caused by other external factors which lead to dry basins in the southwestern and northeastern ends of the BRZ (Mats, 1993). Such change in the stress field is not fully constrained by observations and it has not been considered in our model.

4.3. Validation of modeling results against basin subsidence

The two numerical experiments M450 and M550 predict different evolution of the rift-related sedimentary graben, which resembles the observed structure at the BRZ.

Most available seismic reflection profiles at the BRZ are from the Central and the North Baikal basins (Colman et al., 1996; Hutchinson et al., 1992). The thickest sedimentary sequences are up to 9–10 km in the south and central Baikal basin depocenters (Hutchinson et al., 1992) as predicted by the M550 model (Fig. 5b). Across the Central Baikal basin (Fig. 5d), both the proto- and middle-rift sequences show clear half-graben features with sediment thickness increasing westwards from the eastern flank, whereas the modern-rift deposits slightly thicken from west to east. For comparison of the numerical results with the observed sedimentary sequences, we divide the stratigraphy into three groups (Fig. 5b): the first (0–20 Myr), second (20–28 Myr) and third rift stage (28–31 Myr). The first and second rift stages show clear features of half-graben formation (Fig. 5b), although sediments at the first stage may have been intensively stretched at the bottom by a later extension-related uplift after 28 Myr (Figs. 3e,

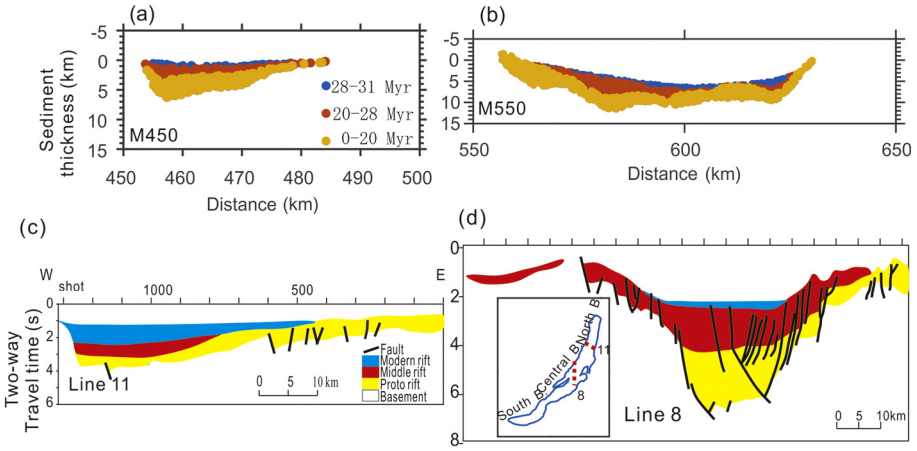

Fig. 5. Sediment thickness predicted in numerical models (a and b) and observed seismic stratigraphic sequences (c and d). Model M550 demonstrates depocenter migration at 28–31 Myr whereas model M450 shows no depocenter migration and preserves the same shape of a half-graben throughout basin evolution (a and b). Interpretation of two migrated multichannel seismic reflection lines (insert box after Hutchinson et al., 1992) across the North and Central Baikal basin are shown in c and d. Line 8 (d) shows clear depocenter migration from the Middle to the Modern rift stage, similar to results for model M550, while Line 11 (c) across the North basin shows no depocenter migration similar to results for model M450. (For interpretation of the references to color in this figure, the reader is referred to the web version of this article.)

4e and 5f). The thickness of the deposits at the last stage (Fig. 5b) also slightly increases from the craton (left) towards the orogenic belt. The change in the location of the deposition center from west to east is caused by migration of the main fault from the predefined fault at the first stage to new faults that developed towards the eastern flank (Fig. 3d, e and f). This kind of movement of the deformation center is consistent with the present seismicity which is localized at the eastern flank of Lake Baikal (Petit and Deverchere, 2006). The M450 model is consistent with seismic profiles across the North Baikal basin which show a 4–5 km thick sedimentary layer in the depocenter (Figs. 4a, 5a and 5c). The basin has a half graben shape for all three stages with one clear master fault throughout the evolution and without depocenter migration.

5. Discussion

5.1. Pre-existing fault in the BRZ

The role of a pre-existing fault in forming a narrow and deep graben at the BRZ has been tested by analogue models (Corti et al., 2011). Models without weak zones between the craton and the orogenic belt tend to produce wide rifted zones that are ~300 km wide, whereas the BRZ graben is only 40–80 km wide. A near vertical suture zone facilitates large vertical throw on the master fault and formation of deep depressions with limited horizontal extension.

One may ask why rifting develops in the thick continent lithosphere rather than in the thinner orogenic lithosphere for M450? First, we note that if the preset fault is located inside the craton interior (or if the fault is underlain by a thick and strong cratonic lithospheric mantle), rifting will start in the orogenic lithosphere, but not in the transitional zone between the craton and the orogenic belt. Second, the lithosphere beneath the preset fault in model M450 is 150 km thick which is thinner than the ca. 200 km thick cratonic lithosphere (Fig. 3a). Therefore, the fault can still localize crustal deformation when extension is applied on the right orogenic side. We present results for a friction coefficient of 0.3 but we also tested values of 0.4 and 0.5, for which we observe similar localization of crustal deformation. It means that an extremely weak fault is not a prerequisite for rift basin formation in M450.

5.2. Lower crust shear zone

In both models, the lithospheric mantle directly beneath surface rift graben is too strong to extend; and instead it is the thinner lithosphere further to the east (right) that is weak enough to extend (Fig. 3). The offset in extension is accommodated by a horizontal shear zone in the lower crust, which transfers the extension from the shallow BRZ crust in the west to the sub-crustal lithosphere in the east. The layered rheology is a feature of the model that allows for, or at least promote the formation of this lower-crust shear zone to accommodate this west-to-east shift. In M450 the lower-crustal (horizontal) shear zone extends much further than in M550 (Fig. 3c and 3f), because it must accommodate a much greater offset between the BRZ and the sub-crustal extension zone. The corresponding melting zone is thus much further away from the BRZ.

The essential element of the model is the ability of the lower crust to shear horizontally and offset the shallow (BRZ) and deep-lithosphere extension regimes. This combined with the relative position of the shallow fault and the craton transition zone leads to the different offsets between the BRZ and melting zone. To test whether removing the weak lower crust leads to qualitatively different results, we simulate the M450 model with ultramafic rheology (olivine) for the lower crust and keep all other parameters unchanged. The results (not shown in figure) demonstrate that no horizontal shear zone develops and rifting only occurs in the thin orogenic lithosphere both at surface and that the mantle part of the lithosphere extends directly below the surface expression of the rift zone. In this situation, volcanism occurs in the surface rift zone.

5.3. Dynamics of the magma

The results of the numerical modeling for the spatial distribution of magmatism in the BRZ suggest that the M450 model represents the northern part of the BRZ, and the M550 model has features of the southern part of the BRZ. The offset of melting is caused by the offset in the zone of sub-crustal extension. This offset of sub-crustal rifting is related to the relative position of the shallow crustal fault to the craton transition. This explains the off-rift eruption of basaltic volcanoes in the Vitim province. These observations are consistent with observations in the Kenya, Ethiopian and Rhine Graben rift zones where magmatism occurs in the immediate vicinity of the rift zone above

thin and weak lithosphere (Birt et al., 1997; Brun et al., 1992; Mackenzie et al., 2005).

Within the BRZ, silica-rich magma only erupted in the Udokan volcanic field at the northeastern end of the rift system (Fig. 1). Most of the erupted volcanic rocks have alkaline and tholeiitic composition and originated in the mantle. It means that magma was transported directly to the surface without significant crustal contamination (Kiselev et al., 1987).

We explain the 200-km offset of the magmatism from the rift center by the location of the pre-existing fault with respect to the geometry of the deepening of the lithosphere base that influences the zone of sub-crustal rifting. Could it alternatively be explained by lateral melt migration within the lithosphere? Most of the magma in mid-ocean spreading centers is generated in a narrow rift zone and since the melt zone is much wider than the rift axis, molten material must be laterally channeled towards the rift center. It means that there may be an impermeable layer overlying the molten zone which causes the dilation of the matrix below (Sparks and Parmentier, 1991). This impermeable layer is likely to be at the lithosphere base, which in our model slopes upward towards the orogenic belt. Therefore, it is impossible for the melt to migrate back to the rift center which forms above the thick and strong lithosphere. If the melt is generated beneath the orogenic belt more than 200 km away from the rift axis, as for the M450 model, both buoyancy forces and viscous mantle flow tend to transfer the melt material up to the orogenic belt (Fig. 3a, b and c). Further, molten material may also transfer through cracks in the lithosphere. To check this, we track the maximum extensional principle stress which is perpendicular to the fracture plane (Fig. 4). All the stress fields surrounding the molten material in the mantle demonstrate vertical fracture planes, such that the buoyancy forces should vertically transfer the melt to the surface. Further, the deformation pattern in the M450 model (Fig. 3c) shows that the lithosphere above the molten zone is much more strained in the orogenic belt than in regions close to the rift graben ($x = 500$–650 km). The high strain rate indicates high stress which tends to facilitate opening of magma-filled fractures. In contrast, the M550 model shows a connected main deformation zone between the rift graben and the mantle upwelling (Fig. 3f). Therefore, the molten material can occur both under the graben and its flanks, such is seen in the Tunka basin and the Khamar-Daban plateau (Fig. 1).

Our numerical results predict offset of sub-crustal extension and very slight mantle upwelling beneath the central to northern Lake Baikal (ascent velocity <0.2 mm yr^{-1} in M450) and intensive asthenosphere ascent beneath the southern Lake Baikal and the Khamar-Daban area (ascent velocity >3 mm yr^{-1} in M550). The deformed sedimentary layer in the M550 model at the basin bottom can develop as the topographic response to passive mantle upwelling at the transitional lithosphere of the craton to orogen zone on the orogenic side, whereas the intact half graben in the M450 model shows no intensive mantle upwelling directly beneath the rift axis corresponding to the northern BRZ. Seismic tomography models show low V_p and V_s interpreted as high temperature in the upper mantle beneath the southern BRZ, although similar models are controversial for the northern and central parts of BRZ (Gao et al., 2003; Zhao et al., 2006). The northern part of the South Baikal basin shows no low Pn velocity anomaly beneath the rift zone, suggesting there is no high-temperature anomaly in the uppermost mantle (Nielsen and Thybo, 2009; Thybo and Nielsen, 2009). Our modeling results show no significant temperature increase at Moho for M450, which is consistent with the high-resolution regional seismic observations.

6. Conclusions

By application of a new numerical code, we examine how the location of pre-existing faults controls the volume and location of rift-related magmatism. The spatial-temporal patterns of mantle magmatism and crustal deformation predicted by our models are consistent with observations in the Baikal Rift Zone. Our modeling results explain the variable locations of volcanism around BRZ by the pre-existing geometry of the lithospheric base and the relative position of a pre-existing fault.

I. In case the pre-existing fault is close to the craton edge (M450), and the weak zone in the crust is underlain by a thick and strong lithospheric mantle, the asthenosphere ascent and the mantle melting zone are shifted into the orogenic belt by more than 200 km from the fault. This geometry is similar to observations around the North and the Central Baikal Rift Zone, where a broad shallow graben is formed. A horizontal shear zone in the lower crust develops and transfers the extension from the shallow BRZ crust in the west to the sub-crustal, mantle lithosphere in the east.
II. In case the pre-existing fault is located close to the orogenic belt (M550), such that the fault overlies a relatively thinner and weaker mantle than in M450, magma intrusion and eruption occurs in the immediate vicinity of the rift zone and a deep and narrow graben is formed. These characteristics are similar to observations in the southern Baikal Rift Zone, where small scale volcanic activity is observed in the Tunka basin and a major magmatic batholith has been interpreted in the lower crust.
III. We conclude that the position of the pre-existing fault zones with respect to the structure of the lithosphere controls the regional tecto-magmatic evolution along the rift. Rift-related magmatism tends to be shifted toward weak lithosphere when the pre-existing fault zone occurs above thick lithosphere, whereas magmatism occurs in the rift zone when the pre-existing fault zone occurs above thin and weak lithosphere.

Acknowledgements

HY was funded by the Danish Government Scholarships. Funding of ZC's positions was received through grants FNU-10-083081 and DFF-1323-00053 (Denmark) to IMA which are gratefully acknowledged. HT acknowledges DFF funding grant DFF-4002-00138B. ZC thanks G. Iaffaldano for helpful discussions. HY also thanks Q. Wang in Nanjing University for suggestions on lower crust rheology and L. Moresi in Melbourne University for inspiring discussion on magma migration. Reviews by G. Ito and an anonymous reviewer helped to improve the manuscript.

References

Artemieva, I.M., 2009. The continental lithosphere: reconciling thermal, seismic, and petrologic data. Lithos 109, 23–46.
Artemieva, I.M., Mooney, W.D., 2001. Thermal thickness and evolution of Precambrian lithosphere: a global study. J. Geophys. Res., Solid Earth 106, 16387–16414.
Bialas, R.W., Buck, W.R., Qin, R., 2010. How much magma is required to rift a continent? Earth Planet. Sci. Lett. 292, 68–78.
Birt, C.S., Maguire, P.K.H., Khan, M.A., Thybo, H., Keller, G.R., Patel, J., 1997. The influence of pre-existing structures on the evolution of the southern Kenya Rift Valley – evidence from seismic and gravity studies. Tectonophysics 278, 211–242.
Bosworth, W., 1987. Off-axis volcanism in the Gregory Rift, East-Africa – implications for models of Continental Rifting. Geology 15, 397–400.
Brun, J.P., Gutscher, M.A., Blum, R., Bois, C., Burg, J.P., Colletta, B., Durbaum, H., Damotte, B., Durst, H., Fuchs, K., Grohmann, N., Hubner, M., Karcher, T., Kessler, G., Klockner, M., Lucazeau, F., Luschen, E., Marthelot, J.M., Meier, L., Ravat, M., Reichert, C., Vernassa, S., Villemin, T., Wenzel, F., Wittlinger, G., 1992. Deep crustal structure of the Rhine Graben from DEKORP-ECORS seismic-reflection data – a summary. Tectonophysics 208, 139–147.

Buck, W.R., 2006. The role of magma in the development of the Afro-Arabian Rift System. In: Afar Volcanic Province Within the East African Rift System, vol. 259, pp. 43–54.
Buck, W.R., Lavier, L.L., Poliakov, A.N., 1999. How to make a rift wide. Philos. Trans. R. Soc. Lond. Ser. A Math. Phys. Eng. Sci., 671–689.
Byerlee, J., 1978. Friction of rocks. Pure Appl. Geophys. 116, 615–626.
Calais, E., Lesne, O., Deverchere, J., San'kov, V., Lukhnev, A., Miroshnitchenko, A., Buddo, V., Levi, K., Zalutzky, V., Bashkuev, Y., 1998. Crustal deformation in the Baikal rift from GPS measurements. Geophys. Res. Lett. 25, 4003–4006.
Cherepanova, Y., Artemieva, I.M., Thybo, H., Chemia, Z., 2013. Crustal structure of the Siberian craton and the West Siberian basin: an appraisal of existing seismic data. Tectonophysics 609, 154–183.
Clauser, C., Huenges, E., 1995. Thermal conductivity of rocks and minerals. In: Rock Physics & Phase Relations: A Handbook of Physical Constants, pp. 105–126.
Colman, S.M., Foster, D.S., Hatton, J., 1996. High-Resolution Seismic-Reflection Surveys of Lake Baikal, Siberia, 1990–1992. US Dept. of the Interior, Geological Survey.
Corti, G., Calignano, E., Petit, C., Sani, F., 2011. Controls of lithospheric structure and plate kinematics on rift architecture and evolution: an experimental modeling of the Baikal rift. Tectonics 30.
Crameri, F., Schmeling, H., Golabek, G.J., Duretz, T., Orendt, R., Buiter, S.J.H., May, D.A., Kaus, B.J.P., Gerya, T.V., Tackley, P.J., 2012. A comparison of numerical surface topography calculations in geodynamic modelling: an evaluation of the 'sticky air' method. Geophys. J. Int. 189, 38–54.
Crisp, J.A., 1984. Rates of magma emplacement and volcanic output. J. Volcanol. Geotherm. Res. 20, 177–211.
Deverchere, J., Petit, C., Gileva, N., Radziminovitch, N., Melnikova, V., San'kov, V., 2001. Depth distribution of earthquakes in the Baikal rift system and its implications for the rheology of the lithosphere. Geophys. J. Int. 146, 714–730.
Doucet, L.S., Peslier, A.H., Ionov, D.A., Brandon, A.D., Golovin, A.V., Goncharov, A.G., Ashchepkov, I.V., 2014. High water contents in the Siberian cratonic mantle linked to metasomatism: an FTIR study of Udachnaya peridotite xenoliths. Geochim. Cosmochim. Acta 137, 159–187.
Ellis, M., King, G., 1991. Structural control of flank volcanism in continental rifts. Science 254, 839–842.
Emmerson, B., Jackson, J., McKenzie, D., Priestley, K., 2006. Seismicity, structure and rheology of the lithosphere in the Lake Baikal region. Geophys. J. Int. 167, 1233–1272.
Gao, S.S., Liu, K.H., Davis, P.M., Slack, P.D., Zorin, Y.A., Mordvinova, V.V., Kozhevnikov, V.M., 2003. Evidence for small-scale mantle convection in the upper mantle beneath the Baikal Rift Zone. J. Geophys. Res., Solid Earth 108.
Gerya, T., 2009. Introduction to Numerical Geodynamic Modelling.
Gerya, T.V., Burg, J.P., 2007. Intrusion of ultramafic magmatic bodies into the continental crust: numerical simulation. Phys. Earth Planet. Inter. 160, 124–142.
Hirth, G., Kohlstedt, D.L., 1996. Water in the oceanic upper mantle: implications for rheology, melt extraction and the evolution of the lithosphere. Earth Planet. Sci. Lett. 144, 93–108.
Hirth, G., Kohlstedt, D., 2003. Rheology of the upper mantle and the mantle wedge: a view from the experimentalists. In: Inside the Subduction Factory. American Geophysical Union, pp. 83–105.
Hutchinson, D.R., Golmshtok, A.J., Zonenshain, L.P., Moore, T.C., Scholz, C.A., Klitgord, K.D., 1992. Depositional and tectonic framework of the rift basins of lake Baikal from multichannel seismic data. Geology 20, 589–592.
Johnson, J.S., Gibson, S.A., Thompson, R.N., Nowell, G.M., 2005. Volcanism in the Vitim Volcanic Field, Siberia: geochemical evidence for a mantle plume beneath the Baikal Rift Zone. J. Petrol. 46, 1309–1344.
Katz, R.F., Spiegelman, M., Langmuir, C.H., 2003. A new parameterization of hydrous mantle melting. Geochem. Geophys. Geosyst. 4.
Kaus, B.J.P., Becker, T.W., 2008. A numerical study on the effects of surface boundary condition and rheology on slab dynamics. Geology 34, 893–896.
Kiselev, A.I., Golovko, H.A., Medvedev, M.E., 1987. Petrochemistry of Cenozoic basalts and associated rocks in Baikal Rift Zone. Tectonophysics 45, 49–59.
Konnikov, E.G., Gibsher, A.S., Izokh, A.E., Sklyarov, E.V., Khain, E.V., 1993. Paleogeodynamics of late Precambrian for Baikal–Muya and Sayan–Tuva–Mongolia segments of the Central Asian fold belt. In: Proceedings of the 4th International Symposium of IGCP Project 283: Geodynamic Evolution of the Paleo-Asian Ocean, pp. 88–90.
Kooi, H., Beaumont, C., 1994. Escarpment evolution on high-elevation rifted margins – insights derived from a surface processes model that combines diffusion, advection, and reaction. J. Geophys. Res., Solid Earth 99, 12191–12209.
Lavier, L.L., Buck, W.R., Poliakov, A.N.B., 2000. Factors controlling normal fault offset in an ideal brittle layer. J. Geophys. Res., Solid Earth 105, 23431–23442.
Logatchev, N.A., Florensov, N.A., 1978. The Baikal system of rift valleys. Tectonophysics 45, 1–13.
Logatchev, N.A., Zorin, Y.A., 1987. Evidence and causes of the 2-stage development of the Baikal Rift. Tectonophysics 143, 225–234.
Logatchev, N.A., Zorin, Y.A., 1992. Baikal Rift Zone: structure and geodynamics. Tectonophysics 208, 273–286.
Maccaferri, F., Rivalta, E., Keir, D., Acocella, V., 2014. Off-rift volcanism in rift zones determined by crustal unloading. Nat. Geosci. 7, 297–300.
Mackenzie, G.D., Thybo, H., Maguire, P.K.H., 2005. Crustal velocity structure across the Main Ethiopian Rift: results from two-dimensional wide-angle seismic modelling. Geophys. J. Int. 162, 994–1006.
Mats, V.D., 1993. The structure and development of the Baikal Rift depression. Earth-Sci. Rev. 34, 81–118.
Mckenzie, D., Bickle, M.J., 1988. The volume and composition of melt generated by extension of the lithosphere. J. Petrol. 29, 625–679.
Nielsen, C., Thybo, H., 2009. No moho uplift below the Baikal Rift Zone: evidence from a seismic refraction profile across southern Lake Baikal. J. Geophys. Res., Solid Earth 114.
Petit, C., Deverchere, J., 2006. Structure and evolution of the Baikal rift: a synthesis. Geochem. Geophys. Geosyst. 7.
Petit, C., Koulakov, I., Deverchere, J., 1998. Velocity structure around the Baikal Rift Zone from teleseismic and local earthquake traveltimes and geodynamic implications. Tectonophysics 296, 125–144.
Ranalli, G., 1995. Rheology of the Earth. Springer Science & Business Media.
Reid, I., Jackson, H.R., 1981. Oceanic spreading rate and crustal thickness. Mar. Geophys. Res. 5, 165–172.
Sherman, S.I., 1978. Faults of the Baikal Rift Zone. Tectonophysics 45, 31–39.
Sparks, D.W., Parmentier, E.M., 1991. Melt extraction from the mantle beneath spreading centers. Earth Planet. Sci. Lett. 105, 368–377.
Thybo, H., Nielsen, C.A., 2009. Magma-compensated crustal thinning in continental rift zones. Nature 457, 873–876.
Wang, Q., 2010. A review of water contents and ductile deformation mechanisms of olivine implications for the lithosphere–asthenosphere boundary of continents. Lithos 120, 30–41.
Wang, Y.F., Zhang, J.F., Jin, Z.M., Green, H.W., 2012. Mafic granulite rheology: implications for a weak continental lower crust. Earth Planet. Sci. Lett. 353, 99–107.
Zhao, D.P., Lei, J.S., Inoue, T., Yamada, A., Gao, S.S., 2006. Deep structure and origin of the Baikal Rift Zone. Earth Planet. Sci. Lett. 243, 681–691.